
STAIC REGULARIZATION FOR SPATIO-TEMPORAL IMAGE RECONSTRUCTION

A PREPRINT

Deepak G Skariah
Department of Electrical Engineering
IISc
Bengaluru, 560012
deepaks@iisc.ac.in

Muthuvel Arigovindan
Department of Electrical Engineering
IISc
Bengaluru, 560012
mvel@iisc.ac.in

ABSTRACT

We propose a regularization-based image restoration scheme for 2D images recorded over time (2D+t). We design an infimal convolution-based regularization function which we call spatio-temporal Adaptive Infimal Convolution (STAIC) regularization. We formulate the infimal convolution in the form of an additive decomposition of the 2D+t image such that the extent of spatial and temporal smoothing is controlled in a spatially and temporally varying manner. This makes the regularization adaptable to the local characteristics of the motion leading to an improved ability to handle noise. We also develop a minimization method for image reconstruction by using the proposed form of regularization. We demonstrate the effectiveness of the proposed regularization using TIRF images recorded over time and compare with some selected existing regularizations.

Keywords Spatio-Temporal · Regularization · Restoration

1 Introduction

Image restoration is an inverse problem Katsaggelos [1989] where a higher quality image estimate is generated from a corrupted observation by exploiting knowledge of image statistics. Regularization methods Engl et al. [1996] constitute an important category among methods for biomedical image restoration Rangayyan [2004]. Imaging modalities where regularization methods have been successful in restoration of corrupted images include MRI Ramani et al. [2012], Viswanath et al. [2020], Widefield Microscopy Arigovindan [2013], Li et al. [2018] and Total Internal Reflection (TIRF) Microscopy Fan et al. [2019] among others. Regularization involves formulating the required restored image g_{opt} as a minimizer of a cost function involving the observed image m . The cost is formulated as a sum of a data fitting term $G(g, m)$ and a regularization term $R(g)$ resulting in the following minimization problem:

$$g_{opt} = \underset{g}{\operatorname{argmin}} G(g, m) + \lambda R(g) \quad (1)$$

where λ is the regularization parameter which controls the relative weighting of regularization term against the data fitting term in the overall cost. The choice of data fitting term $G(g, m)$ is dependent on the image formation forward-model. The regularization term enforces any prior we have about the class of images we are trying to restore often in the form of some image regularity condition.

Regularization functional $R(g)$ is primarily designed based on study of image statistics, while some are data driven designs as observed in learning based methods. Image statistics often depend on imaging modality and the type of objects being imaged. One of the earliest successful regularization function for restoration of natural images is Total Variation. Total Variation, more specifically, first-order total variation (TV-1) is defined as the sum of absolute values of image derivatives along image directions. It works on the principle that discrete natural images have a limited amount of variation which is captured via the first-order derivatives along the two image dimensions. For bio-medical imaging modalities often a better choice is second-order Total Variation (TV-2) where the sum of second-order derivatives along the two image dimensions are employed instead of the first order ones. Replacing first-order derivatives with the

second-order ones leads to more natural intensity variation in the reconstructed images Lefkimmatis et al. [2011]. A generalization of TV-2 known as Hessian-Schatten regularization (HS) was successfully employed for the restoration of biological images Lefkimmatis et al. [2013]. HS regularization employed Schatten norm on the image Hessian. HS regularization and its variants have been successfully applied in a wide variety of imaging forward models including natural images and biological images.

Further developments led to more complex forms of regularization. Among these, two forms are prominent in the literature: (i) sum of norms regularization Lindsten et al. [2011] and (ii) infimal decomposition-based regularization Holler and Kunisch [2014]. Both approaches multiple types of derivatives, but they are fundamentally different in the way the multiple order are combined, which leads to a significant difference in the performance. In the first approach, $R(g)$ takes the form:

$$R(g) = \lambda_1 R_1(g) + \lambda_2 R_2(g) \quad (2)$$

where R_1 and R_2 are the functions capturing different priors based on different types of derivatives. This will produce a reconstruction that balances regularity assumptions enforced by R_1 and R_2 [COTV]. Unfortunately, this balancing is global in the sense that we can control only the overall agreement of the solution to the priors captured by the terms R_1 and R_2 . Real images have non-stationary statistics, and hence it will be more advantageous to combine different terms in a spatially adaptive manner. This can be accomplished by, for example, making the weights λ_1 and λ_2 spatially varying, i.e., by making it vary from pixel to pixel. In this case, the weights λ_1 and λ_2 themselves become images and determining these images along with the required image becomes a challenge. This problem can also be handled by an auxiliary regularization Viswanath et al. [2020]. The main problem in this approach is that the overall cost becomes non-convex.

The second approach is based on infimal convolution Holler and Kunisch [2014]. Here the regularization functional $R(g)$ itself is defined by a minimization problem. Infimal convolution based regularization functional $R(g)$ takes the following form:

$$R(g) = \min_{v_1+v_2=g} R_1(v_1) + R_2(v_2) \quad (3)$$

Here v_1 and v_2 are auxiliary variables satisfying the condition that $v_1 + v_2 = g$. Note that here too, $R(g)$ is defined as a sum of two functions R_1 and R_2 . But this time, R_1 acts on a variable v_1 and R_2 acts on a variable v_2 where $v_1 + v_2 = g$. In the presence of data-fitting cost that is defined on the sum $g = v_1 + v_2$, minimization with respect to v_1 and v_2 leads to spatial adaptivity; the relative influence of R_1 and R_2 is determined adaptively in a spatially varying manner depending on the spatial structure of the input image m . Hence we get an effect that is similar to the method of Viswanath et al. [2020] with an advantage that the cost here is convex. An additional advantage is that this formulation has a higher extent of adaptivity: it is possible to get a solution in which either R_1 or R_2 has no influence at all in some spatial locations depending on the local structure in m such that overall distortion is minimized. Total Generalized Variation (TGV) Guo et al. [2014], Bredies et al. [2010] is the most popular regularization designed using this concept and is used successfully in restoration of MRI images.

More recently learning based methods have been applied successfully to restoration of images from a wide variety of imaging modalities. These belong to the class of deep learning based methods where the image prior is represented by using Convolution Neural networks. These methods use end to end learning based methods or use of CNN networks as a prior for regularization-based image restoration Ulyanov et al. [2018]. In microscopy it has been applied in restoration of 2D images. It has also been applied to other image analysis problems in microscopy as well. Xing et al. [2017], von Chamier et al. [2021], Liu et al. [2021]. The disadvantages of using learning in microscopy image analysis has been discussed in Hoffman et al. [2021].

A related category of inverse problems is restoration of spatio-temporal 2D images observed over time. Even though a spatio-temporal image is simply a sequence of 2D images, the following are the disadvantages of applying 2D image restoration for each time-point independently: (i) temporal correlation is ignored leading to poorer quality of restored images; (ii) temporal continuity is lost in the restored images Holler and Kunisch [2014]. Due to the inherent need for imposing regularity in both time and space, spatio-temporal image restoration demands for the employment of sum of norms or infimal decomposition based construction of the regularization functional. In the sum-of-norms based construction, a weighted sum of two terms as given in the equation (2) is typically used [ref]: (i) the first term applies spatial regularization on each time point of the image sequence; (ii) the second term enforces temporal smoothing for each pixel independently. We will call such construction the combined spatio-temporal regularization (CST). In infimal decomposition approach, a form as given in the equation Equation (3) is used. Here both the terms use spatial and temporal derivatives, but, they differ by the relative weight applied to the temporal derivatives. This method was called the Infimal Convolution Total Variation (ICTV), and we will refer this methods as ICTV-2DT. ICTV-2DT regularization has been successfully applied in biomedical imaging modalities such as dynamic MRISchloegl et al. [2017] and SPECT imaging Zhang et al. [2018]. Among other regularization based approaches, low rank sparse decomposition based model for dynamic MRI reconstruction Trémouilhéac et al. [2014] is the most well known. In MRI more recently deep

learning based methods have been proposed. For restoration of real world video signals deep neural network based algorithms have been proposed. More recently RNN networks had been proposed for dynamic MRI reconstruction Chen et al. [2022].

In this work, we develop a novel spatio-temporal regularization based on infimal convolution employing two terms as done in ICTV-2DT. However, our regularization significantly differs from ICTV-2DT in how spatial and temporal derivatives as distributed among the two terms. We construct the form of each term to make the overall regularization suitable for restoration of 2D fluorescence images recorded as a function of time. We call the novel regularization the Spatio-Temporal Adaptive Infimal Convolution (STAIC) regularization. We also develop a computational algorithm for dynamic image restoration by using the STAIC regularization, and demonstrates the usefulness of our method using simulation experiments. The paper is organized as follows. In section Section 2, we introduce the notations and mathematical preliminaries. In section Section 3, we describe the important existing regularization approaches to deal with spatio-temporal signal restoration problems. In section Section 4, we introduce the proposed STAIC regularization. In section Section 5, we present the STAIC regularized reconstruction as a convex optimization problem, and describe how we solve the optimization problem using the ADMM approach. In section Section 6, we solve the ADMM sub-problems that arise out of the reconstruction problem in more detail. Finally in Section 7, we validate the utility of STAIC regularization.

2 Notations and mathematical preliminaries

1. Images are represented by lower case English alphabets. For example g .
2. In the discussion we will use the idea of vector valued images often refereed to as vector images. Vector images are discrete 2D arrays where each pixel location has a vector quantity. It is denoted by lower-case bold-faced letter with a bold-faced lower-case letter as an argument. For example, $\mathbf{v}(\mathbf{r})$ is a vector image with $\mathbf{r} = [x \ y]^T$ representing a 2D pixel location. Depending on the context, the symbol denoting the pixel location may be omitted.
3. For a vector image, $\mathbf{v}(\mathbf{r})$, $\|\mathbf{v}\|_{1,2}$ denotes $\|\mathbf{v}\|_{1,2} = \sum_{\mathbf{r}} \|\mathbf{v}(\mathbf{r})\|_2$. It is the sum of pixel-wise l_2 norms, where $\sum_{\mathbf{r}}$ denotes the sum across pixel indices. The bound of sum is the first to last pixel location in this notation. The norm $\|\mathbf{v}\|_{1,2}$ is a composition of norms and is often refereed to as a mixed norm.
4. In a scalar image having multiple frames, we use the subscript notation to refer to a particular frame number. Example g_i refers to frame number i of the spatio-temporal image g .
5. Index \mathbf{r} is used to refer to a spatio-temporal image (2DT). Index \mathbf{k} is used to refer to a 2D image. Let $\delta(\mathbf{k})$ and $\delta(\mathbf{r})$ represent 2D and 3D Kronecker delta respectively.
6. $\|\mathbf{g}\|_{1,\kappa} = \sum_{\mathbf{r}} \|\mathbf{g}(\mathbf{r})\|_{\kappa}$ with the definition of $\|\mathbf{y}\|_{\kappa} = \sqrt{\kappa^2(y_1^2 + y_2^2) + y_3^2}$. Further we have that $\|\mathbf{g}\|_{1,1/\kappa} = \sum_{\mathbf{r}} \|\mathbf{g}(\mathbf{r})\|_{1/\kappa}$ and $\|\mathbf{x}\|_{1/\kappa} = \sqrt{y_1^2 + y_2^2 + \kappa^2 y_3^2}$. Here κ is a parameter.
7. $\bar{d}_{xx}(\mathbf{k}), \bar{d}_{xy}(\mathbf{k}), \bar{d}_{yy}(\mathbf{k})$ are discrete filters implementing 2D second order derivatives. In addition $d_{xx}(\mathbf{r}), d_{xy}(\mathbf{r}), d_{xt}(\mathbf{r}), d_{yy}(\mathbf{r}), d_{yt}(\mathbf{r}), d_{tt}(\mathbf{r})$ are discrete filters implementing the 3D second order derivatives.
8. $M(\mathbf{r})$ is the 3D Hessian operator encapsulating all the second order derivative operators where the directions are (x, y, t)

3 Related methods in detail

Before discussing related work, it is important to understand the expected behavior from an ideal spatio-temporal regularization function. In regions with motion, regularization function must be able to discourage temporal smoothing. In regions without motion, temporal smoothing must be promoted. All existing approaches to regularization for this inverse problem is trying to achieve this ideal behavior in some way or the other. This is possible only if the regularization function $R(g)$ is powerful enough to differentiate between regions with motion and regions without motion. This points towards the need to incorporate both spatial and temporal derivatives in the design of regularization function. The presence of temporal derivatives also ensures that such functions operate differently to classical image regularization methods when employed in the resultant optimization problem.

Early methods that consider temporal derivatives together with spatial derivatives constructed the overall regularization as a simple weighted sum of functionals constructed using spatial and temporal derivative independently. This sum of norm based spatio-temporal regularization which we called Combined Spatio-Temporal (CST) is defined as :

$$R_{CST}(g) = \|\mathcal{M} * g\|_{1,2} + \|d_{tt} * g\|_{1,2} \quad (4)$$

where \mathcal{M} is the second order Hessian operator in 3D and D_{tt} is second order derivative along time dimension. In restoration of spatio-temporal signals, R_{CST} is known not to satisfy the desirable properties of an ideal spatio-temporal regularization stated above. One disadvantage of the above formulation is that it is blind to the fact that characteristics of motion varies spatially and temporally, and there is no spatially and temporal varying trade-off between spatial and temporal derivatives. In regions with motion both components will have nontrivial contribution to overall cost leading temporal smoothing which is undesirable. In regions without motion spatial smoothing occurs in addition to temporal smoothing which is again undesirable. This shortcoming prompted design of spatio-temporal regularization employing the infimal decomposition approach as done in the ICTV-2DT method introduced before. Let $g(\mathbf{r})$ be the discrete candidate spatio-temporal (2D+time) image, where $\mathbf{r} = [x \ y \ t]^T$ is the discrete 3D pixel index. Assume that image $g(\mathbf{r})$ is of dimensions $n_1 \times n_2 \times n_F$ where n_F is the number of frames (2D images). Hence each frame is of dimension $n_1 \times n_2$. The regularization is constructed in the form of minimization as given below:

$$R_{ICTV}(g) = \min_v \|\mathcal{S}_{\kappa_1} \nabla(g - v)\|_{1, \kappa_1} + \|\mathcal{S}_{\kappa_2} \nabla(v)\|_{1, \kappa_2}, \quad (5)$$

where $\mathcal{S}_{\kappa} = \text{diag}(\kappa, \kappa, 1)$ and ∇ is the 3D gradient operator. Here κ_1 and κ_2 are user parameters that determines relative weight between spatial and temporal derivatives. It may be noted that the method requires tuning for κ_1 and κ_2 in addition to the tuning of the overall weight λ . This form has the advantage over CST in the same way as the form introduced in the equation (2) has an advantage over the form in the equation (3). In other words, combining two different types of sub-functional in the form of infimal convolution is always advantageous over a simple weighted. However, ICTV-2DT still has a disadvantage. This can be understood by analyzing its effect on regions with motion and without motion. In regions with motion, it will be desirable to eliminate temporal smoothing completely, but, ICTV-2DT does not do so. Similarly, in regions without motion, it will be desirable to eliminate spatial smoothing completely, but, ICTV-2DT does not do so. The reason is that both sub-functional have both temporal and spatial derivatives and, they differ only by the relative weight between spatial and temporal derivatives. Further, it uses first order derivatives which is again undesirable.

4 Spatio-Temporal Adaptive Infimal Convolution (STAIC) Regularization for 2DT image restoration

We propose STAIC regularization for spatio-temporal images by removing the disadvantages of ICTV-2DT while strengthening the design to cater to unique features of 2DT fluorescence images. Let $g_i(\mathbf{k})$ represent the i^{th} frame of the spatio-temporal image $g(\mathbf{r})$ where $\mathbf{k} = [x \ y]^T$ is the discrete 2D pixel index. Consider two linear operators $A(\mathbf{k})$ and $M(\mathbf{r})$ defined as follows :

$$A(\mathbf{k}) = \begin{bmatrix} \bar{d}_{xx}(\mathbf{k}) \\ \bar{d}_{xy}(\mathbf{k}) \\ \bar{d}_{yx}(\mathbf{k}) \\ \bar{d}_{yy}(\mathbf{k}) \\ \delta(\mathbf{k}) \end{bmatrix}, M(\mathbf{r}) = \begin{bmatrix} d_{xx}(\mathbf{r}) & d_{xy}(\mathbf{r}) & d_{xt}(\mathbf{r}) \\ d_{yx}(\mathbf{r}) & d_{yy}(\mathbf{r}) & d_{yt}(\mathbf{r}) \\ d_{tx}(\mathbf{r}) & d_{ty}(\mathbf{r}) & d_{tt}(\mathbf{r}) \end{bmatrix}$$

Next, we define the following components, which act on 2DT images:

$$\bar{R}_1(u_i) = \|A * u_i\|_{1,2} \quad (6)$$

$$R_2(v) = \|(M * v)\|_{1,F} \quad (7)$$

Here u and v are 2DT images, and u_i is the i^{th} 2D time frame of of the 2DT image u . Note that $\|A * u_i\|_{1,2} = \sum_{\mathbf{k}} \|(A * u_i)(\mathbf{k})\|_2 = \sum_{\mathbf{k}} \sqrt{((\bar{d}_{xx} * u_i)(\mathbf{k}))^2 + 2((\bar{d}_{xy} * u_i)(\mathbf{k}))^2 + ((\bar{d}_{yy} * u_i)(\mathbf{k}))^2 + (u_i(\mathbf{k}))^2}$. This is a modified 2D second order TV applied on u_i , where the modification is simply the addition of the intensity term. Next, we note that $R_2(v)$ computes the 3D second-order TV applied on the 2DT sequence v .

The proposed STAIC regularization is defined as follows :

$$S(g, \alpha_s, \alpha_t) = \min_v \alpha_s R_1(g, v) + \alpha_t R_2(v)$$

where $R_1(g, v) = \sum_{i=1}^{n_F} \bar{R}_1(g_i - v_i)$. The user defined parameters α_s, α_t helps control the relative strength of $R_1(\cdot, \cdot)$ and $R_2(\cdot)$ in the regularization function $S(g, \alpha_s, \alpha_t)$.

Despite the role of v as an auxiliary variable in the definition of regularization, the component v is regularized to have finite amount of variations in its 3D structure. This is achieved by constraining the Frobenius norm of 3D second order derivatives. This reflects our desire to ensure that v also resemble a realistic spatio-temporal signal. In the first term

$R_1(g, v)$, we put a constraint on spatial regularity of the difference signal by incorporating an intensity term in addition to the spatial derivative term. This combination of derivatives and pixel intensity promotes the presence of blob-like structure in the restored image. Such image features are often encountered in fluorescence microscopy images which is desirable in our setting due to the TIRF microscopy origin of our signal of interest.

To understand the effect of the two terms on the overall regularization function, it is important to consider regions with motion and without motion separately.

- In regions with motion, v will tend to be zero, and so only R_1 comes into play; this means that there will be negligible temporal smoothing, which will reduce motion blurring
- In regions without motion, v will tend to be close to g so that only R_2 come into play; since R_2 imposes 3D smoothing, this lead to robust noise removal

It may be noted that the design of R_1 in STAIC removes an important drawback of ICTV-2DT in regions with motion. STAIC due to the presence of only spatial derivatives in its R_1 term discourages temporal smoothing completely in regions with motion. This is an important feature as it avoids motion blurring in the final image estimate. In addition, a crucial design change is the presence of a pure intensity term $g - v$ in the R_1 term. This is done due the following reasons :

- We target our method of restoration fluorescence images; fluorescence microscopy images often have images exhibiting a blob like pattern which is promoted by the presence of intensity term
- In addition the intensity term help promote sparsity of regions with motion in turn helping remove micro motions which are often the artifacts caused by Poisson nature of noise. This helps in recovering all large and small motions while removing any spurious motion in the signal.

In addition, STAIC formulations also do not employ any parameter to control the relative strength of spatial and temporal derivatives by virtue of its design leaving us one less parameter to tune. In summary,(i) the redesigned design of purely spatial term R_1 (ii) intensity augmentation of R_1 helps us achieve the goal of designing a regularization scheme that has close to ideal spatio-temporal behavior in regions with motion and without it with limited number of parameters. This ensures that the reconstruction is closer to the ground truth in terms of both spatial and temporal features.

5 Signal Reconstruction Using STAIC regularization

5.1 The Cost Function

Let h denote the 2D impulse response of the microscope. The noise model in fluorescence images is modeled to be mixed Poisson-Gaussian where a signal corrupted by Poisson noise is subject to an additive Gaussian noise. The generation of measured image m is therefore modeled as follows:

$$m = \mathcal{P}(h * g) + \eta$$

where \mathcal{P} is the operator representing Poisson process, η represents the additive Gaussian noise, m represents the observed noisy blurred image and g represents the ground truth image. The data fitting term is often chosen to be the maximum likelihood estimate of the noise model. But we choose the least squares data fitting term due to ease of optimization Arigovindan et al. [2013]. The data fitting term is

$$G(h, g, m) = \frac{1}{2} \sum_{i=1}^{n_F} \|(h * g_i) - m_i\|_F^2 \quad (8)$$

It may be noted that the blurring happens frame wise as we are considering a 2D signal observed over time. The STAIC regularized image reconstruction optimization problem can be expressed as

$$g_{opt} = \underset{g}{\operatorname{argmin}} G(h, g, m) + S(g, \alpha_s, \alpha_t) \quad (9)$$

By observing that the regularization functional $S(g, \alpha_s, \alpha_t)$ is defined as an optimization problem over variable v , we can express the reconstruction problem as:

$$(g_{opt}, v_{opt}) = \underset{g, v}{\operatorname{argmin}} G(h, g, m) + \bar{S}(g, v, \alpha_s, \alpha_t) \quad (10)$$

$$\text{where } \bar{S}(g, v, \alpha_s, \alpha_t) = \alpha_s R_1(g, v) + \alpha_t R_2(v)$$

resulting in an optimization problem in 2 variables g and v . This is possible because, the variable v do not appear in the data fitting term enabling it to be moved to the outer optimization step. We introduce a variable (vector image) $\mathbf{f}(\mathbf{r}) = [g(\mathbf{r}) \ v(\mathbf{r})]^\top$ concatenating the two variables in the above optimization problem to enable a simpler restatement of the cost of optimization. To this end we define the following new linear operators :

$$\mathbf{h} = [h(\mathbf{k}) \ 0],$$

$$\mathbf{T}_s = \begin{bmatrix} d_{xx}(\mathbf{k}) & 0 \\ d_{xy}(\mathbf{k}) & 0 \\ d_{yx}(\mathbf{k}) & 0 \\ d_{yy}(\mathbf{k}) & 0 \\ \delta(\mathbf{k}) & 0 \\ 0 & d_{xx}(\mathbf{k}) \\ 0 & d_{xy}(\mathbf{k}) \\ 0 & d_{yx}(\mathbf{k}) \\ 0 & d_{yy}(\mathbf{k}) \\ 0 & \delta(\mathbf{k}) \end{bmatrix} \quad \text{and} \quad \mathbf{T}_t = \begin{bmatrix} 0 & d_{xx}(\mathbf{r}) \\ 0 & d_{yy}(\mathbf{r}) \\ 0 & d_{xy}(\mathbf{r}) \\ 0 & d_{yx}(\mathbf{r}) \\ 0 & d_{xt}(\mathbf{r}) \\ 0 & d_{tx}(\mathbf{r}) \\ 0 & d_{yt}(\mathbf{r}) \\ 0 & d_{ty}(\mathbf{r}) \\ 0 & d_{tt}(\mathbf{r}) \end{bmatrix}$$

$$A_s = \begin{bmatrix} 1/\sqrt{2} & 0 & 0 & 0 & 0 & -1/\sqrt{2} & 0 & 0 & 0 & 0 \\ 0 & 1/\sqrt{2} & 0 & 0 & 0 & 0 & -1/\sqrt{2} & 0 & 0 & 0 \\ 0 & 0 & 1/\sqrt{2} & 0 & 0 & 0 & 0 & -1/\sqrt{2} & 0 & 0 \\ 0 & 0 & 0 & 1/\sqrt{2} & 0 & 0 & 0 & 0 & -1/\sqrt{2} & 0 \\ 0 & 0 & 0 & 0 & 1/\sqrt{2} & 0 & 0 & 0 & 0 & -1/\sqrt{2} \end{bmatrix} \quad (11)$$

The optimization problem in (10) can now be reformulated in terms of \mathbf{f} only as :

$$J(\mathbf{f}, \alpha_s, \alpha_t) = \frac{1}{2} \sum_{i=1}^{n_F} \|\mathbf{h} * \mathbf{f}_i - m_i\|_F^2 + \sqrt{2}\alpha_s \sum_{i=1}^{n_F} \sum_{\mathbf{k}} \|A_s((\mathbf{T}_s * \mathbf{f}_i)(\mathbf{k}))\|_2 + \alpha_t \sum_{\mathbf{r}} \|(\mathbf{T}_t * \mathbf{f})(\mathbf{r})\|_2 + \mathcal{B}_C(\mathbf{f}) \quad (12)$$

Here, the additional term $\mathcal{B}_C(\cdot)$ is added to impose bound constraint on \mathbf{f} which restrict the range of pixel values \mathbf{f} can take. This helps impose commonly used non-negativity condition on pixel values. Here $\mathcal{B}_C(\cdot)$ is defined as follows

$$\mathcal{B}_C(\mathbf{f}) = \begin{cases} 0 & \text{if } \mathbf{f} \in \mathcal{C} \\ \infty & \text{otherwise} \end{cases} \quad (13)$$

Here $\mathcal{C} = \{\mathbf{f} \mid lb \leq \mathbf{f}(\mathbf{r}) \leq ub \ \forall \mathbf{r}\}$ where lb and ub represents the smallest and highest permitted pixel values. The new image restoration optimization problem over variable \mathbf{f} now takes the form :

$$\mathbf{f}_{opt} = \underset{\mathbf{f}}{\operatorname{argmin}} \ J(\mathbf{f}, \alpha_s, \alpha_t) \quad (14)$$

5.2 Proposed ADMM Method

The cost $J(\mathbf{f}, \alpha_s, \alpha_t)$ to be minimized is a convex function in variable \mathbf{f} . We propose to design an algorithm to minimize the cost by employing the Alternating Direction Method of Multipliers (ADMM) Boyd et al. [2011] algorithmic framework. ADMM framework is most suited for minimizing convex cost under linear equality constraints. Our original optimization problem in (14) can be reformulated to get an equivalent linearly constrained convex problem. This is done by by introduction of new variables $w_m, \mathbf{w}_s, \mathbf{w}_t$ and \mathbf{w}_b and as a result, the updated problem becomes:

$$\min_{\mathbf{f}, w_m, \mathbf{w}_s, \mathbf{w}_t, \mathbf{w}_b} \quad \frac{1}{2} \sum_{i=1}^{n_F} \|w_{m_i} - m_i\|_F^2 + \sqrt{2}\alpha_s \sum_{i=1}^{n_F} \sum_{\mathbf{k}} \|A_s(\mathbf{w}_{s_i}(\mathbf{k}))\|_2 + \alpha_t \sum_{\mathbf{r}} \|\mathbf{w}_t(\mathbf{r})\|_2 + \mathcal{B}_C(\mathbf{w}_b)$$

subject to $w_{m_i} = \mathbf{h} * \mathbf{f}_i, \ \mathbf{w}_{s_i} = \mathbf{T}_s * \mathbf{f}_i, \ \mathbf{w}_t = \mathbf{T}_t * \mathbf{f}, \ \mathbf{w}_b = \mathbf{f}$

It may be noted that we have converted the unconstrained problem in (14) to a constrained optimization form where all constraints are linear equality constraints. To allow a simpler algorithm statement, we introduce a combined operator \mathbf{T} and a combined vector \mathbf{w} defined as follows :

$$\mathbf{T} = \begin{bmatrix} \mathbf{h}(\mathbf{k}) \\ \mathbf{T}_s(\mathbf{k}) \\ \mathbf{T}_t(\mathbf{r}) \\ \mathbf{e}(\mathbf{r}) \end{bmatrix}, \quad \mathbf{w} = \begin{bmatrix} w_m \\ \mathbf{w}_s \\ \mathbf{w}_t \\ \mathbf{w}_b \end{bmatrix} \quad (15)$$

where $\mathbf{e}(\mathbf{r}) = [\delta(\mathbf{r}) \ \delta(\mathbf{r})]$. Under this definition, $\mathbf{e} * \mathbf{f} = \mathbf{f}$. The linearly constrained problem can now be stated in a compact form as :

$$(\mathbf{f}^*, \mathbf{w}^*) = \underset{\mathbf{f}, \mathbf{w}}{\operatorname{argmin}} R(\mathbf{w}, \alpha_s, \alpha_t) \quad (16)$$

$$\text{subject to} \quad \mathbf{T} * \mathbf{f} = \mathbf{w}$$

where $R(\mathbf{w}, \alpha_s, \alpha_t) = G(w_m, m) + \sqrt{2}\alpha_s \sum_{i=1}^{n_F} \sum_{\mathbf{k}} \|A_s(\mathbf{w}_{s_i}(\mathbf{k}))\|_2 + \alpha_t \sum_{\mathbf{r}} \|\mathbf{w}_t(\mathbf{r})\|_2 + \mathcal{B}_C(\mathbf{w}_b)$ and $G(w_m, m) = \frac{1}{2} \sum_{i=1}^{n_F} \|w_{m_i} - m_i\|_F^2$. The next step in ADMM framework is to construct the Augmented Lagrangian Boyd et al. [2011] $\mathcal{L}(\mathbf{f}, \mathbf{w}, \boldsymbol{\beta}, \alpha_s, \alpha_t)$ of the above linearly constrained cost as:

$$\mathcal{L}(\mathbf{f}, \mathbf{w}, \boldsymbol{\beta}, \alpha_s, \alpha_t) = R(\mathbf{w}, \alpha_s, \alpha_t) + \langle \boldsymbol{\beta}, \mathbf{T} * \mathbf{f} - \mathbf{w} \rangle + \frac{\rho}{2} \|\mathbf{T} * \mathbf{f} - \mathbf{w}\|_2^2 \quad (17)$$

where $\boldsymbol{\beta}$ is the Lagrangian multiplier and ρ is a user supplied ADMM parameter. Here the dimensions of $\boldsymbol{\beta}$ is same as that of \mathbf{w} . Finally, ADMM algorithm involves collection of alternative minimization of sub-problem with respect to variables \mathbf{f} and \mathbf{w} followed by an update step involving variable $\boldsymbol{\beta}$. Assume that $\mathbf{f}^{(k)}, \mathbf{w}^{(k)}, \boldsymbol{\beta}^{(k)}$ are the current estimates, the ADMM algorithm involves the following steps

$$\mathbf{w}^{(k+1)} = \underset{\mathbf{w}}{\operatorname{argmin}} L(\mathbf{f}^{(k)}, \mathbf{w}, \boldsymbol{\beta}^{(k)}, \alpha_s, \alpha_t) \quad (18)$$

$$\mathbf{f}^{(k+1)} = \underset{\mathbf{f}}{\operatorname{argmin}} L(\mathbf{f}, \mathbf{w}^{(k+1)}, \boldsymbol{\beta}^{(k)}, \alpha_s, \alpha_t) \quad (19)$$

$$\text{and } \boldsymbol{\beta}^{(k+1)} = \boldsymbol{\beta}^{(k)} + \rho(\mathbf{T} * \mathbf{f}^{(k+1)} - \mathbf{w}^{(k+1)}) \quad (20)$$

The first two equation involves solving two optimization problems over variables \mathbf{f} and \mathbf{w} respectively which is discussed next.

6 Solving the Sub-problems of ADMM Algorithm

We will now discuss how the sub-problems in (18), and (19) are solved to obtain the intermediate variables $\mathbf{w}^{(k+1)}$ and $\mathbf{f}^{(k+1)}$ that appear in the ADMM iterative scheme.

6.1 The \mathbf{w} problem

The sub-problem in (18) can be equivalently simplified to the following form

$$L_{w,k}(\mathbf{w}, \alpha_s, \alpha_t) = R(\mathbf{w}, \alpha_s, \alpha_t) + \frac{\rho}{2} \|\mathbf{w} - \bar{\mathbf{x}}^{(k)}\|_2^2 \quad (21)$$

$$\text{where } \bar{\mathbf{x}}^{(k)} = \mathbf{T} * \mathbf{f}^{(k)} + \frac{1}{\rho} \boldsymbol{\beta}^{(k)} \quad (22)$$

For cleaner presentation of sub-problems, we introduce the notation $\mathbf{x} = \bar{\mathbf{x}}^{(k)}$ and $\hat{\mathbf{w}} = \mathbf{w}^{(k+1)}$. Since \mathbf{w} is made up of sub vectors $w_m, \mathbf{w}_b, \mathbf{w}_t, \mathbf{w}_s$, we separate the above problem into sub-problems involving constituent variables.

$$w_m\text{-prob.: } \hat{w}_m = \underset{w_m}{\operatorname{argmin}} \underbrace{\frac{\rho}{2} \|x_m - w_m\|_{2,2}^2 + G(w_m, m)}_{\bar{L}_m(w_m, x_m)} \quad (23)$$

$$\mathbf{w}_b\text{-prob.: } \hat{\mathbf{w}}_b = \underset{\mathbf{w}_b}{\operatorname{argmin}} \underbrace{\frac{\rho}{2} \|\mathbf{x}_b - \mathbf{w}_b\|_{2,2}^2 + \mathcal{B}_C(\mathbf{w}_b)}_{\bar{L}_b(\mathbf{w}_b, \mathbf{x}_b)} \quad (24)$$

$$\mathbf{w}_t\text{-prob.: } \hat{\mathbf{w}}_t = \underset{\mathbf{w}_t}{\operatorname{argmin}} \underbrace{\frac{\rho}{2} \|\mathbf{x}_t - \mathbf{w}_t\|_{2,2}^2 + \alpha_t \|\mathbf{w}_t\|_{1,2}}_{\bar{L}_t(\mathbf{w}_t, \mathbf{x}_t, \alpha_t)} \quad (25)$$

$$\mathbf{w}_s\text{-prob.: } \hat{\mathbf{w}}_s = \underset{\mathbf{w}_s}{\operatorname{argmin}} \underbrace{\sum_{i=1}^{n_F} \frac{\rho}{2} \|\mathbf{x}_{s_i} - \mathbf{w}_{s_i}\|_{2,2}^2 + \sqrt{2}\alpha_s \sum_{\mathbf{k}} \|A_s(\mathbf{w}_{s_i}(\mathbf{k}))\|_2}_{\bar{L}_{s_i}(\mathbf{w}_{s_i}, \mathbf{x}_{s_i}, \alpha_s)} \quad (26)$$

6.1.1 Decomposing problems pixel-wise

The cost $\bar{L}_m(w_m, x_m)$ is separable across pixels as shown below:

$$\bar{L}_m(w_m, x_m) = \frac{\rho}{2} \|x_m - w_m\|_{2,2}^2 + G(w_m, m) \quad (27)$$

$$= \frac{\rho}{2} \|x_m - w_m\|_{2,2}^2 + \frac{1}{2} \|w_m - m\|_2^2 \quad (28)$$

$$= \sum_{\mathbf{r}} \underbrace{\frac{\rho}{2} (x_m(\mathbf{r}) - w_m(\mathbf{r}))^2 + \frac{1}{2} (w_m(\mathbf{r}) - m(\mathbf{r}))^2}_{L_m(w_m(\mathbf{r}), x_m(\mathbf{r}))} \quad (29)$$

Hence the pixel wise cost $L_m(w_m(\mathbf{r}), x_m(\mathbf{r}))$ is given by:

$$L_m(w_m(\mathbf{r}), x_m(\mathbf{r})) = \frac{\rho}{2} (x_m(\mathbf{r}) - w_m(\mathbf{r}))^2 + \frac{1}{2} (w_m(\mathbf{r}) - m(\mathbf{r}))^2$$

The cost function $\bar{L}_b(w_b, x_b)$ is separable across 3D pixel index \mathbf{r} because $\mathcal{B}_C(\mathbf{w}_b) = \sum_{\mathbf{r}} \bar{\mathcal{B}}_C(\mathbf{w}_b(\mathbf{r}))$ where

$$\bar{\mathcal{B}}_C(\mathbf{w}_b(\mathbf{r})) = \begin{cases} 0 & \text{if } \mathbf{w}_b(\mathbf{r}) \geq 0 \\ \infty & \text{otherwise} \end{cases} \quad (30)$$

The cost function reformulated as a sum over pixels can be stated as:

$$\bar{L}_b(w_b, x_b) = \sum_{\mathbf{r}} \underbrace{\frac{\rho}{2} (\mathbf{x}_b(\mathbf{r}) - \mathbf{w}_b(\mathbf{r}))^2 + \bar{\mathcal{B}}_C(\mathbf{w}_b(\mathbf{r}))}_{L_b(\mathbf{w}_b(\mathbf{r}), \mathbf{x}_b(\mathbf{r}))} \quad (31)$$

Now $\bar{L}_{s_i}(\mathbf{w}_{s_i}, \mathbf{x}_{s_i}, \alpha_s)$ can be expanded across pixels as follows:

$$\bar{L}_{s_i}(\mathbf{w}_{s_i}, \mathbf{x}_{s_i}, \alpha_s) = \sum_{\mathbf{k}} \underbrace{\frac{\rho}{2} \|\mathbf{x}_{s_i}(\mathbf{k}) - \mathbf{w}_{s_i}(\mathbf{k})\|_2^2 + \sqrt{2}\alpha_s \|A_s \mathbf{w}_{s_i}(\mathbf{k})\|_2}_{L_s(\mathbf{w}_{s_i}(\mathbf{k}), \mathbf{x}_{s_i}(\mathbf{k}), \alpha_s)} \quad (32)$$

Finally, $\bar{L}_t(\mathbf{w}_t, \mathbf{x}_t, \alpha_t)$ can also be expanded across pixels courtesy the use of mixed vector matrix norm

$$\bar{L}_t(\mathbf{w}_t, \mathbf{x}_t, \alpha_t) = \sum_{\mathbf{r}} \underbrace{\frac{\rho}{2} \|\mathbf{x}_t(\mathbf{r}) - \mathbf{w}_t(\mathbf{r})\|_2^2 + \alpha_t \|\mathbf{w}_t(\mathbf{r})\|_2}_{L_t(\mathbf{w}_t(\mathbf{r}), \mathbf{x}_t(\mathbf{r}), \alpha_t)} \quad (33)$$

We have shown so far that all the sub-problems are separable across pixels. Hence the solution to the minimization problems of equations (23), (24), (26), and (25), can be expressed as following:

$$\hat{w}_m(\mathbf{r}) = \underset{z \in \mathbb{R}}{\operatorname{argmin}} L_m(z, x_m(\mathbf{r})), \quad (34)$$

$$\hat{\mathbf{w}}_b(\mathbf{r}) = \underset{z \in \mathbb{R}}{\operatorname{argmin}} L_b(z, \mathbf{x}_b(\mathbf{r})), \quad (35)$$

$$\hat{\mathbf{w}}_{s_i}(\mathbf{k}) = \underset{\mathbf{z} \in \mathbb{R}^{10}}{\operatorname{argmin}} L_s(\mathbf{z}, \mathbf{x}_{s_i}(\mathbf{k}), \alpha_s), \text{ and} \quad (36)$$

$$\hat{\mathbf{w}}_t(\mathbf{r}) = \underset{\mathbf{z} \in \mathbb{R}^9}{\operatorname{argmin}} L_t(\mathbf{z}, \mathbf{x}_t(\mathbf{r}), \alpha_t). \quad (37)$$

6.1.2 Solution to the pixel-wise sub-problems

The solution to the w_m sub-problem is obtained by exploiting the fact that the cost $L_m(z, x_m(\mathbf{r}))$ is a differentiable function. The minima is obtained by finding the stationary point of the cost function and the resultant optimal point $\hat{w}_m(\mathbf{r})$ is:

$$\hat{w}_m(\mathbf{r}) = \frac{\rho x_m(\mathbf{r}) + m(\mathbf{r})}{\rho + 1} \quad (38)$$

The solution to the w_b -problem is also simple, and it is the clipping of the pixels by bound that defines the set \mathcal{C} Parikh et al. [2014]. The optimal point $\hat{w}_b(\mathbf{r})$ as given below:

$$\hat{\mathbf{w}}_b(\mathbf{r}) = \mathbb{P}_{\mathcal{C}}(\mathbf{x}_b(\mathbf{r})), \quad (39)$$

where $\mathbb{P}_{\mathcal{C}}(\cdot)$ denotes the operation of clipping the pixel values within the bounds in definition of \mathcal{C} .

The \mathbf{w}_t sub-problem could be understood as evaluating the well known proximal operator Parikh et al. [2014] of ℓ_2 norm $\frac{\alpha_t}{\rho} \|\cdot\|_2$ at the point $\mathbf{x}_t(\mathbf{r})$. Hence the solution to the \mathbf{w}_t sub-problem is given by

$$\hat{\mathbf{w}}_t(\mathbf{r}) = \operatorname{argmin}_{\mathbf{z} \in \mathbb{R}^9} \frac{\rho}{2} \|\mathbf{x}_t(\mathbf{r}) - \mathbf{z}\|_2^2 + \alpha_t \|\mathbf{z}\|_2 \quad (40)$$

$$= \begin{cases} \left(1 - \frac{\alpha_t}{\rho \|\mathbf{x}_t(\mathbf{r})\|_2}\right) \mathbf{x}_t(\mathbf{r}) & \|\mathbf{x}_t(\mathbf{r})\|_2 \geq \frac{\alpha_t}{\rho} \\ \mathbf{0} & \text{otherwise} \end{cases} \quad (41)$$

The \mathbf{w}_s sub-problem is more complicated as it involves composition of a linear operator with a norm function. The solution of this sub-problem is given by the following lemma:

Lemma 1 *Let $\mathbf{y} \in \mathbb{R}^{10}$. Let $\mathbf{y}_1 \in \mathbb{R}^5$ be its sub-vector with first five entries and $\mathbf{y}_2 \in \mathbb{R}^5$ be its sub-vector with last five entries. The solution of optimization problem $\operatorname{argmin}_{\mathbf{z} \in \mathbb{R}^{10}} \frac{\rho}{2} \|\mathbf{y} - \mathbf{z}\|_2^2 + \sqrt{2}\alpha_s \|A_s \mathbf{z}\|_2$ where A_s is defined in (11) is given by*

$$\mathbf{z}^* = P \begin{bmatrix} \gamma \mathbf{y}_1 \\ \mathbf{y}_2 \end{bmatrix} \quad (42)$$

Here P defined in (52) is the eigenvector matrix of A_s and $\gamma = \max(0, 1 - \frac{\sqrt{2}\alpha_s}{\rho \|\mathbf{y}_1\|_2})$.

The proof of Lemma 1 is given in Appendix A. By applying this lemma, we can conclude that the solution of \mathbf{w}_s sub-problem is as follows:

$$\hat{\mathbf{w}}_{s_i}(\mathbf{k}) = P \begin{bmatrix} \gamma \mathbf{x}_{s_{i1}}(\mathbf{k}) \\ \mathbf{x}_{s_{i2}}(\mathbf{k}) \end{bmatrix} \quad (43)$$

where $\mathbf{x}_{s_{i1}}(\mathbf{k}) \in \mathbb{R}^5$ is the sub-vector of $\mathbf{x}_{s_i}(\mathbf{k})$ with first five entries and $\mathbf{x}_{s_{i2}}(\mathbf{k}) \in \mathbb{R}^5$ is the sub-vector of $\mathbf{x}_{s_i}(\mathbf{k})$ with last five entries.

6.2 The \mathbf{f} sub-problem

$$\mathbf{f}^{(k+1)} = \operatorname{argmin}_{\mathbf{f}} L(\mathbf{f}, \mathbf{w}^{(k+1)}, \boldsymbol{\beta}^{(k)}, \alpha_s, \alpha_t) \quad (44)$$

The sub-problem in variable given in (19) has a simpler form once you ignore all the terms not depending on \mathbf{f} in the optimization problem. The simpler form of \mathbf{f} sub-problem may be stated as follows:

$$\begin{aligned} \mathbf{f}^{(k+1)} &= \operatorname{argmin}_{\mathbf{f}} \frac{1}{2} \|\mathbf{T} * \mathbf{f} - \mathbf{y}^{(k)}\|_2^2 \\ \text{where } \mathbf{y}^{(k)} &= \mathbf{w}^{(k+1)} - \frac{1}{\rho} \boldsymbol{\beta}^{(k)} \end{aligned} \quad (45)$$

For notational convenience, we let $\mathbf{y} = \mathbf{y}^{(k)}$ and $\hat{\mathbf{f}} = \mathbf{f}^{(k+1)}$. Recall that $\mathbf{f}(\mathbf{r}) = [g(\mathbf{r}) \ v(\mathbf{r})]^\top$. From the definition of $\mathbf{T}(\mathbf{r})$ it can be observed that the cost is separable across the components g and v of $\mathbf{f}(\mathbf{r})$. Assume that $\mathbf{y}(\mathbf{r}) = [y_m(\mathbf{r}) \ y_{s,1}(\mathbf{r}) \ y_{s,2}(\mathbf{r}) \ y_{s,3}(\mathbf{r}) \ y_{s,4}(\mathbf{r}) \ y_{s,5}(\mathbf{r}) \ y_{s,6}(\mathbf{r}) \ y_{s,7}(\mathbf{r}) \ y_{s,8}(\mathbf{r}) \ y_{s,9}(\mathbf{r}) \ y_{s,10}(\mathbf{r}) \ y_{t,1}(\mathbf{r}) \ y_{t,2}(\mathbf{r}) \ y_{t,3}(\mathbf{r}) \ y_{t,4}(\mathbf{r}) \ y_{t,5}(\mathbf{r}) \ y_{t,6}(\mathbf{r}) \ y_{t,7}(\mathbf{r}) \ y_{t,8}(\mathbf{r}) \ y_{t,9}(\mathbf{r}) \ y_{b,1}(\mathbf{r}) \ y_{b,2}(\mathbf{r})]^\top$. This simplification is achieved by observing the structure $\mathbf{y}^{(k)}$ it inherits from $\mathbf{w}^{(k+1)}$ and $\boldsymbol{\beta}^{(k)}$. Now the cost separated along g and v is given by:

$$\begin{aligned} \bar{L}_1(g) &= \frac{1}{2} (\|h * g - y_m\|_2^2 + \|d_{xx} * g - y_{s,1}\|_2^2 + \|d_{yy} * g - y_{s,2}\|_2^2 + \\ &\quad \|d_{xy} * g - y_{s,3}\|_2^2 + \|d_{xy} * g - y_{s,4}\|_2^2 + \|g - y_{s,5}\|_2^2 + \|g - y_{b,1}\|_2^2) \end{aligned}$$

$$\begin{aligned} \bar{L}_2(v) = & \frac{1}{2} (\|d_{xx} * v - y_{s,6}\|_2^2 + \|d_{yy} * v - y_{s,7}\|_2^2 + \|d_{xy} * v - y_{s,8}\|_2^2 + \|d_{xy} * v - y_{s,9}\|_2^2 + \\ & \|v - y_{s,10}\|_2^2 + \|d_{xx} * v - y_{t,1}\|_2^2 + \|d_{yy} * v - y_{t,2}\|_2^2 + \|d_{xy} * v - y_{t,3}\|_2^2 + \\ & \|d_{xy} * v - y_{t,4}\|_2^2 + \|d_{yt} * v - y_{t,5}\|_2^2 + \|d_{yt} * v - y_{t,6}\|_2^2 + \|d_{xt} * v - y_{t,7}\|_2^2 + \\ & \|d_{xt} * v - y_{t,8}\|_2^2 + \|d_{tt} * v - y_{t,9}\|_2^2 + \|v - y_{b,2}\|_2^2) \end{aligned}$$

For notational convenience, we let $\mathbf{y} = \mathbf{y}^{(k)}$ and $\hat{\mathbf{f}} = \mathbf{f}^{(k+1)}$. Recall that $\mathbf{f}(\mathbf{r}) = [g(\mathbf{r}) \ v(\mathbf{r})]^\top$. The function $\bar{L}_1(g)$ and $\bar{L}_2(v)$ are quadratic in nature in the variables g and v respectively. The minima of both these functions can be obtained by solving the equations $\nabla_g \bar{L}_1(g) = \mathbf{0}$ and $\nabla_v \bar{L}_2(v) = \mathbf{0}$ respectively. This requires evaluation of the gradient expressions which are given below.

$$\begin{aligned} \nabla_g \bar{L}_1(g) = & \tilde{h} * h * g + \tilde{d}_{xx} * d_{xx} * g + \tilde{d}_{yy} * d_{yy} * g + 2\tilde{d}_{xy} * d_{xy} * g + g \\ & - \tilde{h} * y_m - \tilde{d}_{xx} * y_{s,1} - \tilde{d}_{yy} * y_{s,2} - \tilde{d}_{xy} * y_{s,3} - \tilde{d}_{xy} * y_{s,4} - y_{s,5} - y_{b,1} \end{aligned} \quad (46)$$

$$\begin{aligned} \nabla_v \bar{L}_2(v) = & \tilde{d}_{xx} * d_{xx} * v + \tilde{d}_{yy} * d_{yy} * v + 2\tilde{d}_{xy} * d_{xy} * v + 2v + \tilde{d}_{xt} * d_{xt} * v \\ & + \tilde{d}_{yt} * d_{yt} * v + \tilde{d}_{tt} * d_{tt} * v - \tilde{d}_{xx} * y_{s,5} - \tilde{d}_{yy} * y_{s,6} - \tilde{d}_{xy} * y_{s,7} - \tilde{h} * y_m - y_{s,8} \\ & - \tilde{d}_{xt} * y_{t,1} - \tilde{d}_{yt} * y_{t,2} - \tilde{d}_{tt} * y_{t,3} - \tilde{d}_{xt} * y_{t,4} - \tilde{d}_{yt} * y_{t,5} - \tilde{d}_{tt} * y_{t,6} \end{aligned} \quad (47)$$

This completes the solution of the \mathbf{f} sub-problem which form part of the ADMM iterates.

7 Experiments

To demonstrate the effectiveness of STAIC regularization, we consider restoration of time varying TIRF images, and compare with the method ICTV, 3D-TV2 and CST. We selected five image sequences obtained from a high Numerical Aperture (high bandwidth) TIRF microscope under nearly noise-free conditions, and designate them as the ground truth models. The ground truth models are given in Figure 1. We then simulate measured images by blurring these models with PSF corresponding to low NA systems and by adding mixed Poisson-Gaussian noise as shown below :

$$m = \mathcal{P}(\gamma_p(h * g)) + \eta$$

Here γ_p is a parameter to control the strength of Poisson noise. We consider PSF corresponding to five NA values namely 0.8, 0.9, 1.0, 1.1, and 1.2. We kept the Gaussian noise level fixed, and considered two γ_p values of 1 and 5 to generate the dataset. A higher value of γ_p results in a lower level of Poisson noise corruption. This makes a set of 50 measured image sequences generated from our five ground truth images.

7.1 Experiment 1

In first experiment, we choose to demonstrate the advantages gained by treating restoration of time varying images as a separate problem as opposed to treating them under classical image restoration by treating time as the third dimension. To this end we consider 3D-TV2 regularization based restoration of our dataset of 50 images. The resultant restoration scheme which we call 3D-TV2 is posed as the following optimization problem

$$\hat{g} = \underset{g}{\operatorname{argmin}} \frac{1}{2} \sum_{i=1}^{n_F} \|(h * g_i) - m_i\|_F^2 + \lambda \sum_{\mathbf{r}} \|(M * g)(\mathbf{r})\|_F \quad (48)$$

where $M(\mathbf{r})$ is the 3D Hessian operator defined earlier and λ is the regularization parameter. The algorithm is tuned for λ to obtain the best SNR. The results are presented in Tables 1 and 2 for the two Poisson noise levels $\gamma_p = 1, 5$ respectively along with results of the STAIC scheme. The resultant SNR (in dB) was not found to be competitive in comparison to our STAIC scheme or even other algorithms we used in subsequent experiments. The SSIM scores also demonstrate the shortcomings of this approach. It also demonstrates that we indeed need to treat the time dimension differently by considering temporal variations as a different phenomenon in relation to spatial variations in the TIRF image.

7.2 Experiment 2

In the second set of experiments we compare the performance of proposed STAIC scheme against the Combined Spatio-Temporal Regularization (CST) and Infimal Convolution TV (ICTV-2DT). In CST the measured image is subject to both spatial and temporal regularization by employing a sum of norms regularization. The corresponding image restoration optimization problems using CST regularization takes the form:

$$\operatorname{argmin}_g \frac{1}{2} \sum_{i=1}^{n_F} \|(h * g_i) - m_i\|_F^2 + \lambda R_{CST}(g) \quad (49)$$

In addition, we also generated the restoration results of applying ICTV-2DT regularization scheme. As discussed earlier ICTV belongs to the family of infimal convolution regularization where spatial and temporal components of signal are modeled differently by the regularization. The ICTV-2DT optimization problem takes the form:

$$\operatorname{argmin}_g \frac{1}{2} \sum_{i=1}^{n_F} \|(h * g_i) - m_i\|_F^2 + \lambda R_{ICTV}(g) \quad (50)$$

The results of ICTV-2DT, CST and STAIC are also presented in Tables 1 and 2 for the two Poisson noise levels. Our proposed algorithm STAIC perform better than both CST and ICTV-2DT regularized approaches to restoration for the TIRF 2DT dataset. STAIC was found to result in a higher restoration quality as measured using SNR as well as SSIM which is another popular image quality measure.. It may be noted that SSIM of restored spatio-temporal image presented in both the tables is the average of SSIM values across the image frames. Our STAIC achieves SNR improvement over the second best approach in the range of 0.5 dB to 2 dB in the 50 image dataset considered. This improvement can be attributed to the improved regularization design that captures the prior of temporal component of the signal in comparison to the other algorithms. In SSIM measure too we have a clear gain over the other approaches considered in our experiments.

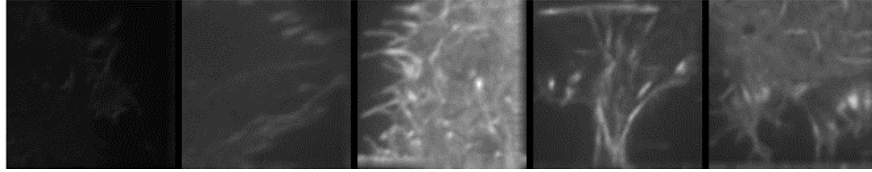


Figure 1: The five original images

8 Conclusion

We proposed a spatio-temporal regularization method for restoration of time varying 2D images. Our design of the regularization terms led to an underlying additive decomposition of the signal enabling differentiated regularization of regions with motion and without motion. The effectiveness of this decomposition is evident in the superior reconstruction quality evaluated by structure similarity as well as signal to noise ratio measures of image quality. Our method was found to perform better than other algorithms each designed using different philosophy towards spatio-temporal signal restoration. This better quality reconstruction was enabled through design of a fast and efficient algorithm for minimizing the resultant regularized cost using the ADMM framework. The proposed algorithms effectiveness can be attributed to the advantages provided by the infimal convolution framework in exploiting correlation across frames inherent to spatio-temporal signals.

A proof

Proof 1 *Let us start by considering the optimization problem*

$$\operatorname{argmin}_{\mathbf{z} \in \mathbb{R}^{10}} L_s(\mathbf{z}, \mathbf{y}, \alpha_s) \quad (51)$$

where $L_s(\mathbf{z}, \mathbf{y}, \alpha_s) = \frac{\rho}{2} \|\mathbf{y} - \mathbf{z}\|_2^2 + \sqrt{2}\alpha_s \|A_s \mathbf{z}\|_2$. Note that $\mathbf{y}, \mathbf{z} \in \mathbb{R}^{10}$.

Consider symmetric matrix $A_s^\top A_s$ which is orthogonally diagonalizable. In other words, we can find an orthogonal matrix of eigenvectors P and a diagonal matrix of eigenvalues D such that $A_s^\top A_s = PDP^\top$.

Image	NA	STAIC		ICTV		CST		3DTV2	
		ssim	snr	ssim	snr	ssim	snr	ssim	snr
5135	0.8	0.853	11.58	0.758	8.84	0.841	8.80	0.656	8.48
	0.9	0.873	13.01	0.781	9.91	0.863	9.86	0.669	9.45
	1	0.887	14.31	0.799	10.84	0.880	10.80	0.677	10.28
	1.1	0.897	15.46	0.812	11.65	0.891	11.61	0.683	10.98
	1.2	0.905	16.54	0.822	12.39	0.901	12.34	0.688	11.60
5142	0.8	0.912	11.88	0.814	10.17	0.886	10.18	0.620	9.96
	0.9	0.926	13.26	0.831	11.30	0.905	11.31	0.629	11.01
	1	0.934	14.52	0.848	12.31	0.918	12.32	0.636	11.94
	1.1	0.942	15.68	0.865	13.21	0.928	13.22	0.640	12.75
	1.2	0.946	16.78	0.876	14.04	0.936	14.05	0.643	13.49
5147	0.8	0.908	12.48	0.901	11.94	0.903	11.95	0.746	11.70
	0.9	0.926	13.67	0.914	13.05	0.921	13.06	0.755	12.73
	1	0.939	14.73	0.914	14.04	0.934	14.05	0.761	13.64
	1.1	0.947	15.70	0.923	14.93	0.943	14.94	0.766	14.44
	1.2	0.954	16.58	0.930	15.74	0.950	15.75	0.769	15.15
5157	0.8	0.874	8.04	0.794	7.28	0.814	7.29	0.615	6.94
	0.9	0.901	9.46	0.835	8.59	0.850	8.60	0.628	8.11
	1	0.919	10.75	0.854	9.76	0.877	9.76	0.638	9.11
	1.1	0.932	11.90	0.844	10.81	0.897	10.79	0.644	9.96
	1.2	0.941	12.96	0.853	11.75	0.912	11.73	0.649	10.70
5158	0.8	0.943	14.38	0.918	13.18	0.927	13.14	0.513	12.00
	0.9	0.954	15.76	0.917	14.37	0.940	14.33	0.519	12.86
	1	0.962	17.02	0.928	15.44	0.949	15.39	0.522	13.58
	1.1	0.967	18.15	0.936	16.38	0.955	16.33	0.524	14.16
	1.2	0.970	19.21	0.941	17.24	0.960	17.18	0.526	14.64

Table 1: The Restoration Quality for Noise Level 1 ($\gamma_p = 1$)

Image	NA	STAIC		ICTV		CST		3DTV2	
		ssim	snr	ssim	snr	ssim	snr	ssim	snr
5135	0.8	0.867	11.60	0.761	8.85	0.857	8.81	0.658	8.48
	0.9	0.889	13.03	0.789	9.91	0.881	9.87	0.671	9.45
	1	0.903	14.34	0.809	10.85	0.898	10.81	0.678	10.28
	1.1	0.914	15.52	0.823	11.68	0.910	11.63	0.684	10.99
	1.2	0.922	16.59	0.835	12.41	0.920	12.36	0.689	11.60
5142	0.8	0.929	11.89	0.892	10.19	0.892	10.18	0.621	9.96
	0.9	0.943	13.28	0.908	11.32	0.911	11.31	0.629	11.01
	1	0.953	14.55	0.920	12.33	0.925	12.32	0.636	11.94
	1.1	0.960	15.72	0.929	13.24	0.936	13.22	0.640	12.75
	1.2	0.966	16.84	0.935	14.08	0.944	14.06	0.643	13.49
5147	0.8	0.914	12.49	0.910	11.95	0.907	11.95	0.746	11.70
	0.9	0.932	13.68	0.924	13.07	0.925	13.06	0.756	12.74
	1	0.945	14.75	0.935	14.06	0.938	14.06	0.762	13.64
	1.1	0.954	15.71	0.942	14.95	0.948	14.94	0.766	14.44
	1.2	0.961	16.60	0.948	15.77	0.955	15.76	0.770	15.15
5157	0.8	0.881	8.04	0.795	7.28	0.815	7.29	0.615	6.94
	0.9	0.908	9.47	0.836	8.59	0.852	8.60	0.628	8.11
	1	0.927	10.76	0.855	9.77	0.879	9.77	0.638	9.12
	1.1	0.940	11.91	0.869	10.81	0.899	10.80	0.644	9.96
	1.2	0.949	12.97	0.854	11.76	0.914	11.73	0.649	10.70
5158	0.8	0.949	14.39	0.927	13.20	0.931	13.14	0.514	12.00
	0.9	0.961	15.78	0.939	14.40	0.945	14.34	0.519	12.86
	1	0.969	17.04	0.947	15.48	0.954	15.40	0.522	13.57
	1.1	0.974	18.19	0.953	16.44	0.960	16.35	0.525	14.16
	1.2	0.978	19.26	0.958	17.30	0.965	17.20	0.526	14.64

Table 2: The Restoration Quality for Noise Level 2 ($\gamma_p = 5$)

Since $A_s^\top A_s$ can be derived from given matrix A_s , we can derive P and D by eigen decomposition and is given below:

$$P = \begin{bmatrix} \frac{1}{\sqrt{2}} & 0 & 0 & 0 & 0 & -\frac{1}{\sqrt{2}} & 0 & 0 & 0 & 0 \\ 0 & \frac{1}{\sqrt{2}} & 0 & 0 & 0 & 0 & -\frac{1}{\sqrt{2}} & 0 & 0 & 0 \\ 0 & 0 & \frac{1}{\sqrt{2}} & 0 & 0 & 0 & 0 & -\frac{1}{\sqrt{2}} & 0 & 0 \\ 0 & 0 & 0 & \frac{1}{\sqrt{2}} & 0 & 0 & 0 & 0 & -\frac{1}{\sqrt{2}} & 0 \\ 0 & 0 & 0 & 0 & \frac{1}{\sqrt{2}} & 0 & 0 & 0 & 0 & -\frac{1}{\sqrt{2}} \\ -\frac{1}{\sqrt{2}} & 0 & 0 & 0 & 0 & \frac{1}{\sqrt{2}} & 0 & 0 & 0 & 0 \\ 0 & -\frac{1}{\sqrt{2}} & 0 & 0 & 0 & 0 & \frac{1}{\sqrt{2}} & 0 & 0 & 0 \\ 0 & 0 & -\frac{1}{\sqrt{2}} & 0 & 0 & 0 & 0 & \frac{1}{\sqrt{2}} & 0 & 0 \\ 0 & 0 & 0 & -\frac{1}{\sqrt{2}} & 0 & 0 & 0 & 0 & \frac{1}{\sqrt{2}} & 0 \\ 0 & 0 & 0 & 0 & -\frac{1}{\sqrt{2}} & 0 & 0 & 0 & 0 & \frac{1}{\sqrt{2}} \end{bmatrix} \text{ and } D = \text{diag}\left(\begin{bmatrix} 1 \\ 1 \\ 1 \\ 1 \\ 1 \\ 0 \\ 0 \\ 0 \\ 0 \\ 0 \end{bmatrix}\right) \quad (52)$$

where diag is the operation that creates a diagonal matrix with its input vector forming the diagonal entries. We define $\hat{\mathbf{z}} = P^\top \mathbf{z}$ and $\hat{\mathbf{y}} = P^\top \mathbf{y}$. Since P is orthogonal, it is also true that $\|P^\top \mathbf{x}\|_2 = \|\mathbf{x}\|_2$. Since $\|\mathbf{x}\|_2 = \sqrt{\langle \mathbf{x}, \mathbf{x} \rangle}$ where $\langle \cdot, \cdot \rangle$ is the standard inner product, it can be seen that

$$\|A_s \mathbf{z}\|_2 = \sqrt{\langle A_s \mathbf{z}, A_s \mathbf{z} \rangle} = \sqrt{\langle \mathbf{z}, A_s^\top A_s \mathbf{z} \rangle} = \sqrt{\mathbf{z}^\top A_s^\top A_s \mathbf{z}} = \sqrt{\mathbf{z}^\top P D P^\top \mathbf{z}} = \sqrt{\hat{\mathbf{z}}^\top D \hat{\mathbf{z}}} \quad (53)$$

Also observe that:

$$\frac{\rho}{2} \|\mathbf{y} - \mathbf{z}\|_2^2 = \frac{\rho}{2} \|P^\top \mathbf{y} - P^\top \mathbf{z}\|_2^2 = \frac{\rho}{2} \|\hat{\mathbf{y}} - \hat{\mathbf{z}}\|_2^2 \quad (54)$$

Let us define $\hat{\mathbf{z}}_1, \hat{\mathbf{z}}_2 \in \mathbb{R}^5$ such that $\hat{\mathbf{z}} = \begin{bmatrix} \hat{\mathbf{z}}_1 \\ \hat{\mathbf{z}}_2 \end{bmatrix}$. Also define $\hat{\mathbf{y}}_1, \hat{\mathbf{y}}_2 \in \mathbb{R}^4$ such that $\hat{\mathbf{y}} = \begin{bmatrix} \hat{\mathbf{y}}_1 \\ \hat{\mathbf{y}}_2 \end{bmatrix}$

The original optimization problem in terms of $\hat{\mathbf{z}}$ is given by

$$\underset{\mathbf{z} \in \mathbb{R}^{10}}{\text{argmin}} \frac{\rho}{2} \|\hat{\mathbf{y}} - \hat{\mathbf{z}}\|_2^2 + \sqrt{2} \alpha_s \sqrt{\hat{\mathbf{z}}^\top D \hat{\mathbf{z}}} \quad (55)$$

By appealing to the sub vectors definition in $\hat{\mathbf{z}}$ and $\hat{\mathbf{y}}$, the problem can be stated as

$$\underset{\hat{\mathbf{z}}_1, \hat{\mathbf{z}}_2 \in \mathbb{R}^5}{\text{argmin}} \frac{\rho}{2} \|\hat{\mathbf{y}}_1 - \hat{\mathbf{z}}_1\|_2^2 + \frac{\rho}{2} \|\hat{\mathbf{y}}_2 - \hat{\mathbf{z}}_2\|_2^2 + \sqrt{2} \alpha_s \|\hat{\mathbf{z}}_1\|_2 \quad (56)$$

By considering two separate optimization problems in $\hat{\mathbf{z}}_1$ and $\hat{\mathbf{z}}_2$, we get

$$\underset{\hat{\mathbf{z}}_1 \in \mathbb{R}^5}{\text{argmin}} \frac{\rho}{2} \|\hat{\mathbf{y}}_1 - \hat{\mathbf{z}}_1\|_2^2 + \sqrt{2} \alpha_s \|\hat{\mathbf{z}}_1\|_2 \quad (57)$$

$$\underset{\hat{\mathbf{z}}_2 \in \mathbb{R}^5}{\text{argmin}} \frac{\rho}{2} \|\hat{\mathbf{y}}_2 - \hat{\mathbf{z}}_2\|_2^2 \quad (58)$$

The optimization problem in variable $\hat{\mathbf{z}}_1$ is simply the proximal operator of ℓ_2 norm which is well known Parikh et al. [2014] and is given by

$$\hat{\mathbf{z}}_1^* = \gamma \hat{\mathbf{y}}_1 \quad (59)$$

where $\gamma = \max(0, 1 - \frac{\sqrt{2} \alpha_s}{\rho \|\hat{\mathbf{y}}_1\|_2})$. The solution of optimization problem in variable $\hat{\mathbf{z}}_2$ is given by $\hat{\mathbf{z}}_2^* = \hat{\mathbf{y}}_2$. Now, we map back to space of variable \mathbf{z} by multiplying with P

$$\mathbf{z}^* = P \hat{\mathbf{z}}^* \quad (60)$$

where $\hat{\mathbf{z}}^* = \begin{bmatrix} \gamma \hat{\mathbf{y}}_1 \\ \hat{\mathbf{y}}_2 \end{bmatrix}$.

References

- Aggelos K Katsaggelos. Iterative image restoration algorithms. *Optical engineering*, 28(7):735–748, 1989.
- Heinz Werner Engl, Martin Hanke, and Andreas Neubauer. *Regularization of inverse problems*, volume 375. Springer Science & Business Media, 1996.
- Rangaraj M Rangayyan. *Biomedical image analysis*. CRC press, 2004.
- Sathish Ramani, Zhihao Liu, Jeffrey Rosen, Jon-Fredrik Nielsen, and Jeffrey A Fessler. Regularization parameter selection for nonlinear iterative image restoration and mri reconstruction using gcv and sure-based methods. *IEEE Transactions on Image Processing*, 21(8):3659–3672, 2012.
- Sanjay Viswanath, Manu Ghulyani, Simon De Beco, Maxime Dahan, and Muthuvel Arigovindan. Image restoration by combined order regularization with optimal spatial adaptation. *IEEE Transactions on Image Processing*, 29: 6315–6329, 2020.
- Muthuvel Arigovindan. Image deconvolution research: its scope and importance in live cell microscopy. *Current Science*, pages 1501–1511, 2013.
- Jizhou Li, Feng Xue, and Thierry Blu. Accurate 3d psf estimation from a wide-field microscopy image. In *2018 IEEE 15th International Symposium on Biomedical Imaging (ISBI 2018)*, pages 501–504. IEEE, 2018.
- Junchao Fan, Xiaoshuai Huang, Liuju Li, Liangyi Chen, and Shan Tan. One-step deconvolution for multi-angle tirf microscopy with enhanced resolution. *Biomedical optics express*, 10(3):1097–1110, 2019.
- Stamatios Lefkimmiatis, Aurélien Bourquard, and Michael Unser. Hessian-based norm regularization for image restoration with biomedical applications. *IEEE Transactions on Image Processing*, 21(3):983–995, 2011.
- Stamatios Lefkimmiatis, John Paul Ward, and Michael Unser. Hessian Schatten-norm regularization for linear inverse problems. *IEEE transactions on image processing*, 22(5):1873–1888, 2013.
- Fredrik Lindsten, Henrik Ohlsson, and Lennart Ljung. Clustering using sum-of-norms regularization: With application to particle filter output computation. In *2011 IEEE Statistical Signal Processing Workshop (SSP)*, pages 201–204. IEEE, 2011.
- Martin Holler and Karl Kunisch. On infimal convolution of tv-type functionals and applications to video and image reconstruction. *SIAM Journal on Imaging Sciences*, 7(4):2258–2300, 2014.
- Weihong Guo, Jing Qin, and Wotao Yin. A new detail-preserving regularization scheme. *SIAM journal on imaging sciences*, 7(2):1309–1334, 2014.
- Kristian Bredies, Karl Kunisch, and Thomas Pock. Total generalized variation. *SIAM Journal on Imaging Sciences*, 3(3):492–526, 2010.
- Dmitry Ulyanov, Andrea Vedaldi, and Victor Lempitsky. Deep image prior. In *Proceedings of the IEEE conference on computer vision and pattern recognition*, pages 9446–9454, 2018.
- Fuyong Xing, Yuanpu Xie, Hai Su, Fujun Liu, and Lin Yang. Deep learning in microscopy image analysis: A survey. *IEEE transactions on neural networks and learning systems*, 29(10):4550–4568, 2017.
- Lucas von Chamier, Romain F Laine, Johanna Jukkala, Christoph Spahn, Daniel Krentzel, Elias Nehme, Martina Lerche, Sara Hernández-Pérez, Pieta K Mattila, Eleni Karinou, et al. Democratizing deep learning for microscopy with zerocostdl4mic. *Nature communications*, 12(1):1–18, 2021.
- Zhichao Liu, Luhong Jin, Jincheng Chen, Qiuyu Fang, Sergey Ablameyko, Zhaozheng Yin, and Yingke Xu. A survey on applications of deep learning in microscopy image analysis. *Computers in Biology and Medicine*, 134:104523, 2021.
- David P Hoffman, Isaac Slavitt, and Casey A Fitzpatrick. The promise and peril of deep learning in microscopy. *Nature methods*, 18(2):131–132, 2021.
- Matthias Schloegl, Martin Holler, Andreas Schwarzl, Kristian Bredies, and Rudolf Stollberger. Infimal convolution of total generalized variation functionals for dynamic mri. *Magnetic resonance in medicine*, 78(1):142–155, 2017.
- Jiahua Zhang, Si Li, Andrzej Krol, C Ross Schmidlein, Edward Lipson, David Feiglin, and Yuesheng Xu. Infimal convolution-based regularization for spect reconstruction. *Medical physics*, 45(12):5397–5410, 2018.
- Benjamin Trémouhéac, Nikolaos Dikaios, David Atkinson, and Simon R Arridge. Dynamic mr image reconstruction–separation from undersampled (k,t)-space via low-rank plus sparse prior. *IEEE transactions on medical imaging*, 33(8):1689–1701, 2014.
- Eric Z Chen, Puyang Wang, Xiao Chen, Terrence Chen, and Shanhui Sun. Pyramid convolutional rnn for mri image reconstruction. *IEEE Transactions on Medical Imaging*, 2022.

Muthuvel Arigovindan, Jennifer C Fung, Daniel Elnatan, Vito Mennella, Yee-Hung Mark Chan, Michael Pollard, Eric Branlund, John W Sedat, and David A Agard. High-resolution restoration of 3d structures from widefield images with extreme low signal-to-noise-ratio. *Proceedings of the National Academy of Sciences*, 110(43):17344–17349, 2013.

Stephen Boyd, Neal Parikh, and Eric Chu. *Distributed optimization and statistical learning via the alternating direction method of multipliers*. Now Publishers Inc, 2011.

Neal Parikh, Stephen Boyd, et al. Proximal algorithms. *Foundations and trends in Optimization*, 1(3):127–239, 2014.